https://doi.org/10.1016/j.buildenv.2023.110236

Large eddy simulation study on pedestrian-level wind environments around elevated walkways and influential factors in ideal urban street canyons

Lan Chen [a], Cheuk Ming Mak [a, *], Jian Hang [b], Yuwei Dai [c], Jianlei Niu [a], Kam Tim Tse [d]

[a] Department of Building Environment and Energy Engineering, The Hong Kong Polytechnic University, Hung Hom, Hong Kong, China

[b] School of Atmospheric Sciences, Sun Yat-sen University and Key Laboratory of Tropical Atmosphere-Ocean System, Ministry of Education, 519000, Zhuhai, China

[c] School of Environment and Architecture, University of Shanghai for Science and Technology, 516 Jungong Road, Shanghai, China

[d] Department of Civil and Environmental Engineering, The Hong Kong University of Science and Technology, Clear Water Bay, Kowloon, Hong Kong, China

***Corresponding author: Cheuk Ming Mak**

Email address: cheuk-ming.mak@polyu.edu.hk.

Abstract

Constructing elevated walkway systems is an effective and prevalent strategy for densely populated cities to improve pedestrian walkability and road safety. Nevertheless, adding an elevated walkway inside the street will inevitably influence the local wind environment, which has rarely been investigated. This study aims to examine the pedestrian-level wind environment around the elevated walkway in three-dimensional (3D) ideal urban street canyons using large eddy simulations. The impacts of street aspect ratio (H/W = 1, 2, 3), elevated walkway width (W_{ew}/W = 0.2, 0.4, 0.6), and sidewall type (open, semi-hermetic, hermetic) on the mean wind velocity and gust wind velocity fields were quantified. Results indicate that the elevated walkway has an adverse effect on the pedestrian-level wind environment. After adding an elevated walkway, the area-averaged mean and gust wind velocities of the target street are decreased, with a maximum rate of over 20% and 30%. Increasing H/W may be positive or negative for the pedestrian-level wind environment, as the overall mean and gust wind velocities do not show monotonic variations with H/W. Extremely wide elevated walkways should be avoided as the pedestrian-level mean and gust wind environments worsen with increased walkway width. Using semi-hermetic or hermetic sidewalls slightly improves the pedestrian-level mean and gust wind environments. This study promotes the knowledge of the impacts of elevated walkways, street aspect ratio, and walkway designs on pedestrian-level mean and gust wind environments, providing a scientific basis for further research.

Keywords: Urban wind, Elevated walkway, Street aspect ratio, Large eddy simulation

1. Introduction

Urban wind environment is closely related to pedestrian comfort and safety, city ventilation, and air quality [1-5]. Traditional wind engineering research focuses on wind danger and safety, for strong wind can cause casualties and economic loss [6, 7]. Wind comfort criteria, such as Melbourne [8], Soligo et al. [9] and NEN 8100 [10], are representatives for addressing this issue. On the other hand, the weak or calm wind is against urban ventilation, impairing the ground-level heat and pollutants dispersion and removal [11]. Cities are becoming more compact due to the booming population and scarce landing resources. As a result, wind weakening frequently occurs in congested urban areas [12], which has been another urgent issue for policymakers and researchers [3]. The wind environment issue is inseparable from people's lives and deserves perpetual concern.

Numerous experimental and numerical studies have been devoted to identifying influential factors for urban wind and the modification mechanisms in various scenarios, from real-world urban areas [6, 13-17] to ideal models [18-23]. The metropolis features varieties of massive building blocks and dense and complicated street networks. Therefore, most of these investigations focus on urban morphology and building-related parameters, such as building frontal area density [17, 18, 23, 24], street aspect ratio (building height/street width) [19, 25-28], building height variation [4, 20, 21, 29], open space [30-34], and building geometry (e.g., configuration, roof type, opening, arcade and lift-up designs, balcony, overhang, and wing wall) [7, 16, 22, 35-46]. In contrast, the influence of other public facilities like elevated expressways (or viaducts) [3, 24] and elevated pedestrian walkways [47-49] on the urban wind environment has not received equal attention, especially the latter.

Elevated walkways or footbridges, which function as improving pedestrian walkability [50], are universal in densely populated metropolises such as New York [47], Calgary [51], Hong Kong [48] (see Fig. 1), and Shanghai [52]. Significantly, although elevated walkways are

similar to expressways in being off the ground and improving congestion, they usually have different users and structures. Elevated walkways are aimed at pedestrians and typically have covers for shelter, while expressways are primarily designed for vehicles and seldom have covers [49]. The benefits of elevated walkways for urban life embody several aspects: first, allowing pedestrians to traverse the road or junction without waiting and being disturbed by mobile vehicles; second, facilitating pedestrians shifting between two isolated constructions without returning to the ground; third, alleviating heavy pedestrian flow on sidewalks; four, mitigating vehicle-pedestrian conflicts and improving pedestrian safety; five, improving urban greening and landscape; six, protecting pedestrian from unfavorable weathers and improving pedestrian comfort [50, 53]. Scientific evidence proved that walking on elevated walkways can reduce pedestrians' pollutant exposure under specific walkway designs [47-49]. Given these advantages, elevated walkways are anticipated to be more prevalent in the future. For example, the number of footbridges in Hong Kong had reached 1,036 by September 2022 and is growing continuously [50]. However, elevated walkways are not necessarily favorable. Yang et al. [52] found that physiological equivalent temperatures (PET) are higher on the open elevated walkway than on the shaded ground in Shanghai. Duan et al. [49] reported that the elevated walkway (perpendicular to the street orientation) decelerates the mean flow below it and may increase pedestrian-level and walkway-level pollutant exposures compared to the no-walkway case in two-dimensional (2D) ideal street canyons. Reviewing the literature shows that research regarding the microenvironment around elevated walkways is insufficient and deserves more dedication. Although elevated walkways share part of pedestrian flow, substantial numbers of pedestrians are still at ground-level sidewalks, especially in business districts. And the urban wind is inextricably linked to other environmental problems. Therefore, understanding impacts of elevated walkways on the pedestrian-level wind environment is of great significance. More investigations and efforts are required to address this issue.

Owing to the rapid advance in computational resources and model performance, the computational fluid dynamics (CFD) simulation has been a powerful alternative to the field measurement and wind tunnel experiment with regard to wind-related studies [54]. The well-recognized advantages of CFD modeling include providing precise whole-flow field information, being convenient for variables-controlling research, saving time and costs, and exempting from similarity constraints [54]. Although the steady Reynolds-averaged Navier-Stokes (RANS) model is the most extensively used turbulence model due to the lower computational cost, large eddy simulation (LES) has received increasing applications in flow and dispersion issues in recent years [55, 56]. This can be attributed to the intrinsic superior performance of LES, growing concern about transient processes, and advances in high-performance computing [56]. Furthermore, validation studies have evaluated computational parameters' influence on the accuracy and reliability of LES, providing useful references for successors [57-59]. Given that the flow field would be highly turbulent and complex around elevated walkways [47], the CFD modeling with LES is more appropriate for capturing its unsteady characteristics.

This study aims to enrich the scientific knowledge of pedestrian-level wind environments around elevated walkways in 3D ideal urban street canyons. In line with the research objective, this study focuses on answering the following research questions: 1) how do elevated walkways influence pedestrian-level mean (or time-averaged) and gust wind environments? 2) how do street aspect ratio, elevated walkway width, and sidewall type (see Fig. 1) impact pedestrian-level mean and gust wind environments? Thus, mean wind velocity and gust wind velocity fields under different cases are simulated via LES. To the best of the authors' knowledge, this is the first study to quantify the impacts of the elevated walkway, street aspect ratio, walkway width, and sidewall types on the pedestrian-level mean and gust wind environments around the elevated walkway. Therefore, this study contributes to the literature on pedestrian-level wind

environments around elevated walkways. Besides, the findings help urban planners and constructors design and construct appropriate elevated walkway frameworks.

The remaining contents will be developed as follows: Section 2 introduces the methodology involving case description and numerical settings; Section 3 first presents a validation study of LES against wind-tunnel data and then quantitatively analyzes and discusses all test results; Section 4 summarizes the main findings and significance of this study and discusses existing limitations and directions for further work.

Fig. 1. Examples of elevated walkways in Hong Kong photographed by authors: (a) Type A−open/steel railing, (b) Type B−semi-hermetic/concrete, (c) Type C−hermetic/glass.

2. Methodology

2.1. Cases description, computational domain, and grid arrangement

As depicted in Fig. 2(a), the ideal urban street canyon model was composed of twenty-one generic buildings aligned in three rows and seven columns. Each block was labeled as $B_{row, column}$. The origin of the coordinate system was located in the ground-level center of B25. The approaching wind was perpendicular to the model, with two main streets in the streamwise direction and six secondary streets in the spanwise direction. The building model was a cuboid with dimensions of length (L) × width (W_b) = 30 m × 20 m. The street width (W) between adjacent buildings was 20 m. Four ideal urban canyon models with different street aspect ratios (H/W = 1, 1.25, 2, and 3) were constructed by varying the building height (H) from 20 m to 60 m. The corresponding frontal area density (λ_f) was 0.3, 0.375, 0.6, and 0.9, respectively.

The elevated walkway was built throughout the fifth secondary street, which was 5.5 m (h_{ew}) above the ground [48, 53] (see Fig. 2(b)). The supporting pillar had a plan area of $l_s \times l_s$ = 1 m^2, located in the middle street. For simplicity, this study did not model elevators, stairways, lifts, and other delicate structures like steel railings and handrails. The main body comprised a 0.5 m–thick floor and a 0.3 m–thick cover, and the interior for pedestrians moving was 3 m high (H_{ew}). This study examined two walkway design parameters: (1) walkway width (W_{ew} = 4, 8, 12 m) and (2) sidewall types (Type A: open sidewall; Type B: semi-hermetic sidewall, Type C: hermetic sidewall). As shown in Fig. 1, Type A represented airy steel railings, while Type B and C were impermeable concrete or glass sidewalls. The height (h_{sw}) of Type B and C sidewalls was 1.1 m and 3 m, respectively. Table 1 summarizes the detailed geometric dimensions of all cases. All urban canyon models were grouped into NW and EW based on whether having an elevated walkway. Cases name follows the uniform format: [model type-H/W, W_{ew}/W, sidewall type]. For instance, Case [NW-1] is a no-walkway model with H = 20 m and H/W = 1; Case [EW-1, 0.4, B] refers to an elevated walkway model with H = 20 m, W_{ew} = 8 m, and semi-hermetic sidewall.

This study used wind-tunnel data of Leitl and Schatzmann [60] to validate the CFD modeling method. The 3 × 7 array of ideal urban street canyon prototypes also originated from Leitl and Schatzmann [60], in which all building models were 0.125 m high (H/W = 1.25) with a model scale of 1: 200. The Reynolds numbers (Re) of presented cases at reduced scale were between 3.7×10^4 and 4.6×10^4, which surpassed the recommended threshold of 1.5×10^4 [61], sufficiently meeting the Re-independence similarity criterion. Accordingly, flow fields based on reduced-scale models can apply to corresponding full-scale cases. Moreover, using reduced-scale models in CFD simulations can reduce considerable computational costs without impairing prediction accuracy [62], which is especially significant for LES. Therefore, this study adopted the same reduced scale as wind tunnel experiments [60] for all CFD simulations.

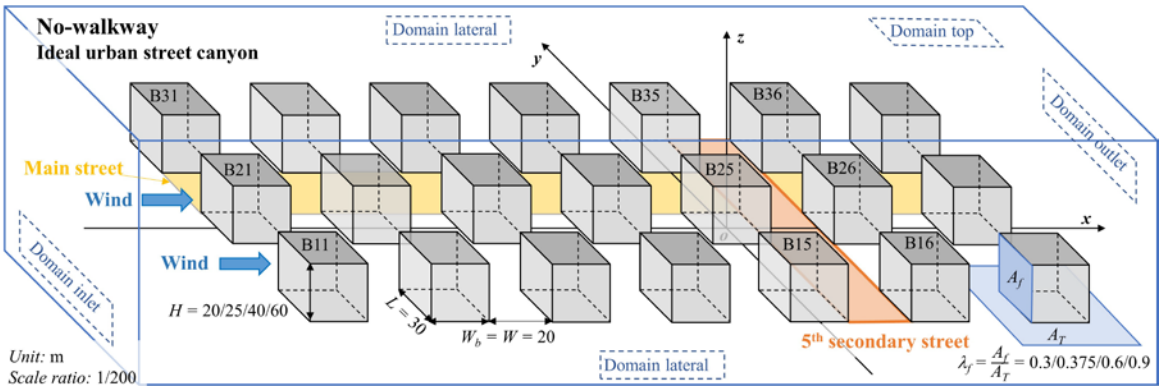

(a)

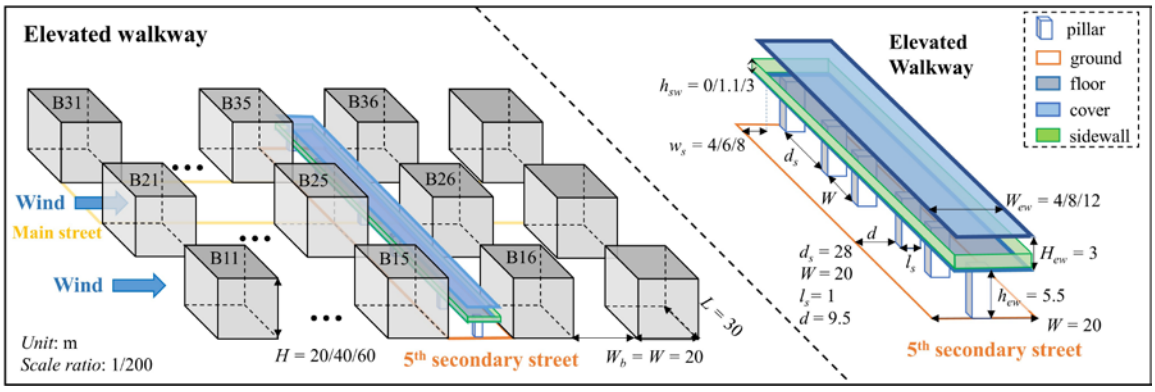

(b)

Fig. 2. Schematic diagrams of (a) no-walkway models and (b) elevated walkway models.

Table 1. Summary of validation and tested cases. (Geometric dimensions are on a prototype scale. * denotes the validation case. EW and NW models differ in whether having elevated walkways. H is the building height, ranging from 20 m to 60 m. W = 20 m is the width of urban canyons.)

Case name [model type-*H/W*, *W*$_{ew}$/*W*, sidewall type]	***H/W***	λ_f	***W*$_{ew}$ (m)**	***h*$_{sw}$ (m)**	**Total number of grids**
Case [NW-1.25] *	1.25	0.375	/	/	6,082,447
Case [NW-1]	1	0.3	/	/	5,894,109
Case [NW-2]	2	0.6	/	/	7,022,295
Case [NW-3]	3	0.9	/	/	8,333,600
Case [EW-1, 0.2, A]	1	0.3	4	/	7,200,796
Case [EW-1, 0.4, A]	1	0.3	8	/	7,234,446

Case [EW-1, 0.6, A]	1	0.3	12	/	7,348,206
Case [EW-1, 0.4, B]	1	0.3	8	1.1	7,546,338
Case [EW-1, 0.4, C]	1	0.3	8	3	7,194,918
Case [EW-2, 0.4, A]	2	0.6	8	/	8,550,508
Case [EW-3, 0.4, A]	3	0.9	8	/	9,438,226

This study followed the best practice guidelines [63, 64] to build the computational domain. Given this, the distances from the outer edge of the urban street canyon model to the domain inlet, outlet, top, and lateral boundaries were 5*H*, 15*H*, 5*H*, and 5*H*, respectively, except that Case [NW-1.25] had the same lateral width as the wind tunnel. According to our previous validation study [58] on wind tunnel experiments of Leitl and Schatzmann [60], a minimum grid resolution of 0.0005 m (i.e., 0.004*H*) is fine enough for the LES model to predict the urban canyon flow field accurately. Therefore, this study adopted 0.0005 m (i.e., 0.0017*H*–0.005*H*) as the minimum grid size for all cases. Each computational domain comprised about 5.9 million to 9.4 million structured hexahedral grids, and the detailed mesh information is listed in Table 1. Fig. 3 illustrates partial mesh arrangements of Case [NW-1] and Case [EW-1, 0.4, B].

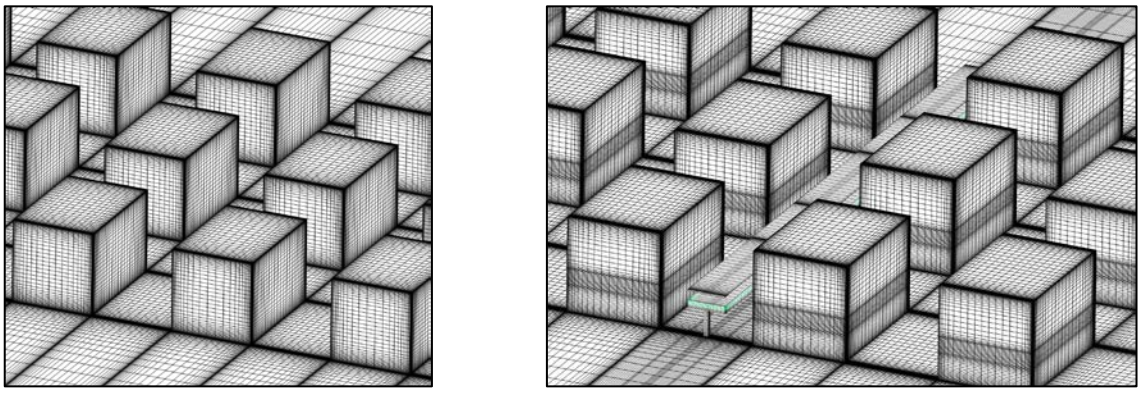

(a) (b)

Fig. 3. Examples of mesh arrangements: (a) Case [NW-1] and (b) Case [EW-1, 0.4, B].

2.2. Boundary conditions, turbulence model, and solution method

All cases were computed using ANSYS Fluent 19.0 [65] on the Tianhe II supercomputer of the National Supercomputer Center in Guangzhou, China. The domain inlet and outlet were

set as velocity-inlet and pressure-outlet boundary conditions, respectively. Profiles of mean wind velocity (U), turbulent kinetic energy (k), and turbulent dissipation rate (ε) for the velocity-inlet boundary were prescribed by Eqs. (1−3), where constants were acquired by fitting wind tunnel data, namely friction velocity $u^* = 0.374$ m/s, roughness length $z_0 = 0.00075$ m, Von Karman constant $\kappa = 0.4187$, $C_1 = 0.025$, $C_2 = 0.41$, and $C_\mu^* = 0.069$ [59].

$$U = \frac{u^*}{\kappa} ln(\frac{z+z_0}{z_0}) \quad (1)$$

$$k = \sqrt{C_1 ln(z+z_0) + C_2} \quad (2)$$

$$\varepsilon = \frac{u^* \sqrt{C_\mu^*}}{\kappa(z+z_0)} \sqrt{C_1 ln(z+z_0) + C_2} \quad (3)$$

To obtain the time-varying velocity-inlet condition in LES, the vortex method with 190 vortices was used to exert stochastic perturbation on the mean velocity profile [58, 65]. Symmetry boundary condition, i.e., zero normal velocity and normal gradients of all variables, was utilized at the domain top and lateral boundaries. The ground and all building surfaces were no-slip walls, and the average non-dimensional distance y^+ of the first near-wall grids was below 4. Thus, enhanced wall treatment associating enhanced wall functions with a two-layer model was applied to resolve the near-wall region.

The governing equations for isothermal incompressible flows were discretized via the finite volume scheme. The simulation procedure involved both RANS and LES models. First, the RNG k-ε model with the SIMPLEC algorithm was employed for all cases to obtain steady flow fields, providing initial conditions for LES. The spatial discretization methods for convection and diffusion terms were second-order-accurate upwind and central-differential schemes, respectively. The convergence of computing was considered to reach when residuals for the continuity, momentum, and turbulence were below 10^{-4} and kept stable for hundreds of

iterations. Then, the Smagorinsky−Lilly model with the PISO algorithm was adopted to model transient flow fields further. The spatial discretization method for convection terms changed to the bounded central-differencing scheme. The second-order implicit formulation was utilized for temporal terms. Our previous validation study regarding wind tunnel experiments of Leitl and Schatzmann [60] has verified that a sampling time length (τ) of 12 s with a time step size (Δt) of 0.005 s is sufficient to generate stable flow and dispersion fields [58]. Therefore, Δt = 0.005 s and τ =12 s were applied to all transient simulations and acquiring mean flow variables. Note that "mean" refers to "time-averaged" in this study unless otherwise stated. The iterations for each time step proceeded until monitoring variables reached stable. Data sampling for results and analysis started after a pre-computing period of 6 s (i.e., 5−11P) to minimize effects of the initial condition. Here, the flow-through period ($P = L_d/U_{ref}$) was defined as the ratio of the domain length (L_d) and the reference velocity (U_{ref} = 6 m/s).

3. Results and discussion

3.1. Validation results

Fig. 4 compares distributions of normalized mean wind velocity (U_{xy}/U_{ref}) and normalized turbulent kinetic energy (k_{xy}/U^2_{ref}) at three horizontal lines between wind tunnel experiments and CFD simulations. U_{ref} is the inlet velocity at the reference height of z = 0.66 m (in model scale), which equals 6.33 m/s in wind tunnel experiments and 6 m/s in CFD simulations. Three horizontal lines are on the horizontal plane of z = 0.5 H = 0.0625 m. As shown in Fig. 4(a-c), LES results generally agree well with wind tunnel data regarding U_{xy}/U_{ref}. Fig. 4(d-f) indicates that LES and wind-tunnel k_{xy}/U^2_{ref} values are in good agreement in the secondary street (y < 0.075 m) but not matched well in the main street (y > 0.075 m), where apparent overestimation can be observed. Three validation metrics, i.e., the fraction of predictions within a factor of two of observations (FAC2), the fraction bias (FB), and the normalized mean square error (NMSE), were computed to quantify the deviation between wind-tunnel and LES data, which are

summarized in Table 2. The positive FB values of U_{xy}/U_{ref} and negative FB values of k_{xy}/U^2_{ref} suggest that LES results generally underestimate mean wind velocity and overestimate turbulent fluctuation, accordant with observing Fig. 4 directly. Nevertheless, the overall deviation is minor as NMSE values are from 0.015 to 0.090. In light of the recommended criterion, an acceptable model necessitates FAC2 > 0.5, |FB| < 0.3, and NMSE < 4 [66-68]. Therefore, in this study, FAC2, FB, and NMSE values for U_{xy}/U_{ref} and k_{xy}/U^2_{ref} are all within acceptable ranges, indicating a satisfactory prediction performance by CFD modeling. In summary, it is successfully justified that the CFD method described in Section 2 can predict the mean flow field and turbulent fluctuation in an ideal urban street canyon with acceptable accuracy. More details of sensitivity tests for the grid arrangement, time step size, and sampling length can be found in our previous study [58].

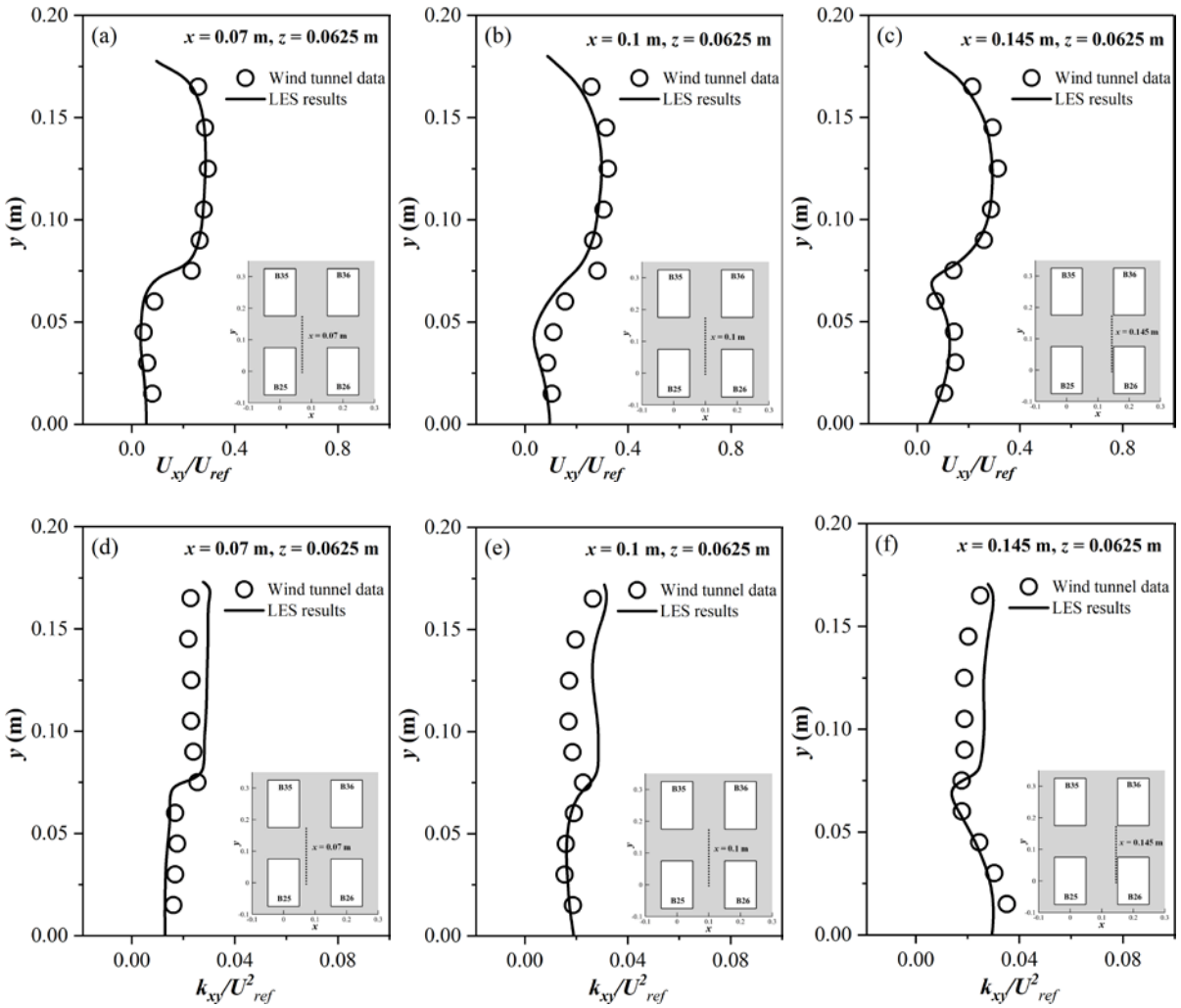

Fig. 4. Comparison of (a-c) normalized mean wind velocity (U_{xy}/U_{ref}) and (d-f) normalized turbulent kinetic energy (k_{xy}/U^2_{ref}) between wind tunnel data and LES results.

Table 2. Summary of validation metrics for wind-tunnel and CFD simulated U_{xy}/U_{ref} and k_{xy}/U^2_{ref} values.

Validation metrics (acceptable range)	U_{xy}/U_{ref}			k_{xy}/U^2_{ref}		
	Fig. 4(a)	Fig. 4(b)	Fig. 4(c)	Fig. 4(d)	Fig. 4(e)	Fig. 4(f)
FB (-0.3 – 0.3)	0.116	0.191	0.102	-0.058	-0.213	-0.101
FAC2 (> 0.5)	1	0.9	1	1	1	1
NMSE (< 4)	0.027	0.053	0.015	0.058	0.090	0.052

3.2. General mean flow characteristics

When placed in a moving viscous fluid, bluff bodies typically alter the trajectory of the approaching flow due to the drag effect. This section is to examine how the elevated walkway influences mean flow regimes. The mean wind velocity ratio (MVR) is the ratio of the mean wind velocity ($\overline{U}$) to the inlet mean velocity at the pedestrian level ($\overline{U}_{2m}$ = 2.4 m/s). This study specifies that the pedestrian level is 2 m (i.e., 0.01 m in model scale) above the ground. Fig. 5 illustrates 3D streamlines of mean flows in Case [NW-1] and Case [EW-1, 0.4, A]. The main streets act as two long “channels” for the approaching flow entering the inner city. 3D clockwise helical flows occupy entire secondary street canyons, entraining air from laterals and roofs. After a flow adjustment over five-column buildings, channel flows are attenuated severely, thus much weaker than external flows outside the model. Overall, introducing an elevated walkway does not break the principally 3D helical vortex structure, retaining downward flows along the windward and upward flows along the leeward.

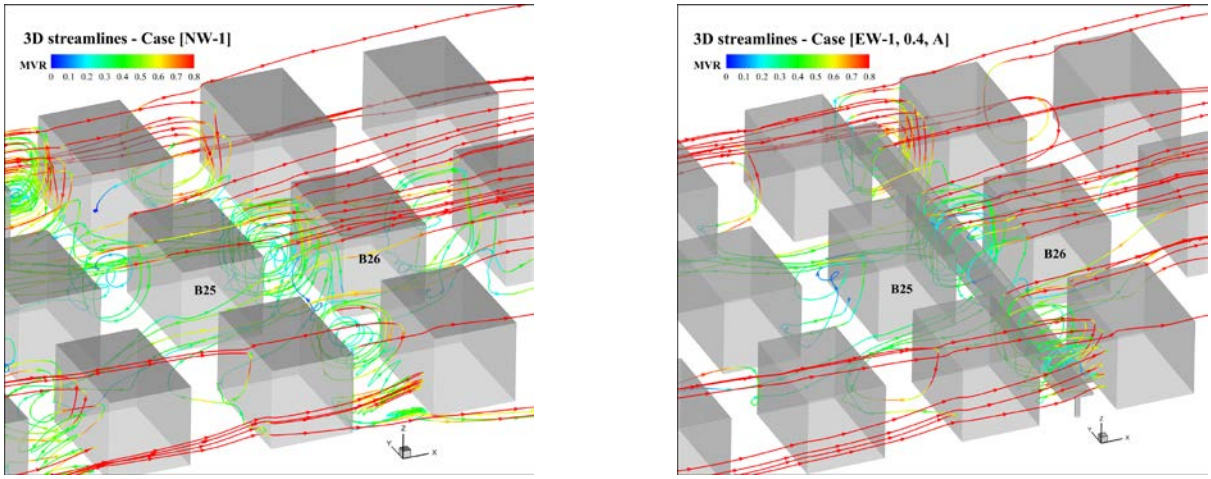

(a) (b)

Fig. 5. 3D streamlines of mean flows in (a) Case [NW-1] and (b) Case [EW-1, 0.4, A].

As the elevated walkway and secondary streets are spanwise, streamwise and vertical velocity components are more influenced. 2D streamlines at streamwise profiles (i.e., XZ-planes) can provide a clearer view of how flow patterns vary due to the elevated walkway. Notably, this study focused on the target street's wind environment because this middle secondary street between B25 and B26 buildings resembled the actual situation more than two side secondary streets. As shown in Fig. 6(a-f), the primary vortex center of Case [NW-1] exists in the upper canyon at y = 0. Then it gradually moves downward till dissipating at the interface between the target street and the main street (i.e., at y = 0.075 m). Fig. 6(g-l) shows that although the primary vortex center of Case [EW-1, 0.4, A] experiences a similar process as Case [NW-1], its evolution is more complex. For 2D XZ-plane flows at the central street (see Fig. 6(g-h)), the elevated walkway deflects the flow near the windward wall and lifts the primary vortex, attenuating flows around and below the walkway. In deep street canyons (H/W = 2, 3), the elevated walkway has little effect on the primary vortex at the upper canyon, restricted by the distance. The primary vortex exists above the elevated walkway at the central street, which is analogous to Duan et al. [49]. In their 2D unite-aspect-ratio street canyon models (H/W = 1), the primary vortex occurs below the walkway when H_{ww}/H = 0.7, exists

above the walkway when H_{ww}/H = 0.3, and disappears when H_{ww}/H = 0.5 [49]. H_{ww} is the distance from the ground to the walkway interior's center. In this study, the biggest H_{ww}/H is 0.375.

For 2D XZ-plane flows away from the central street (see Fig. 6(c-d, i-j)), the primary vortex of Case [NW-1] moves downward but still dominates the entire canyon. In contrast, the primary vortex of Case [EW-1, 0.4, A] severely shrinks and even transforms, with small vortices developing. Meanwhile, the weakening upstream flow no longer dominates the walkway interior, eventually replaced by a downstream flow (see Fig. 6(k-l)). Duan et al. [49] divided the canyon into upper and lower zones by regarding the walkway as a partition and defined effective aspect ratios to predict spatial-averaged walkway-canyon flow regimes. However, as the 2D XZ-plane flow varies along the target street due to a spanwise velocity, the spanwise spatial-averaged flow regime is insufficient to display 3D unite-aspect-ratio street canyon flow characteristics. The effective aspect ratio can only explain the flow regime at the central street. It can be concluded that the effect of adding elevated walkways on the streamwise mean flow regime depends upon the spanwise position at the target street.

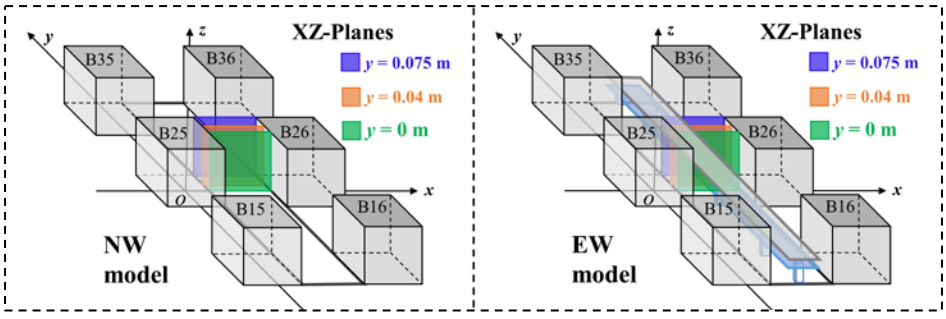

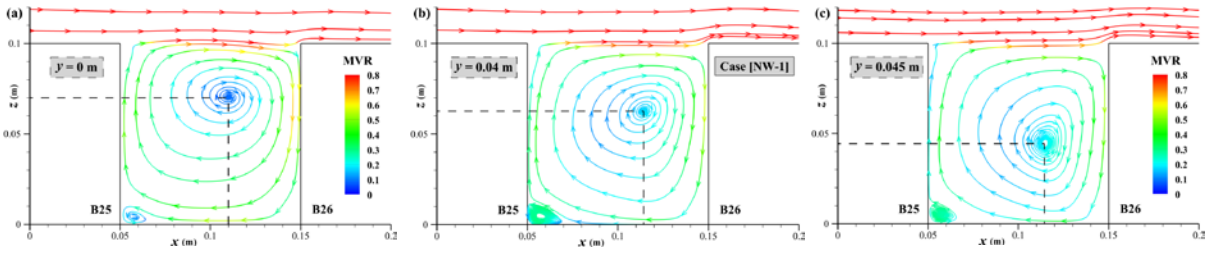

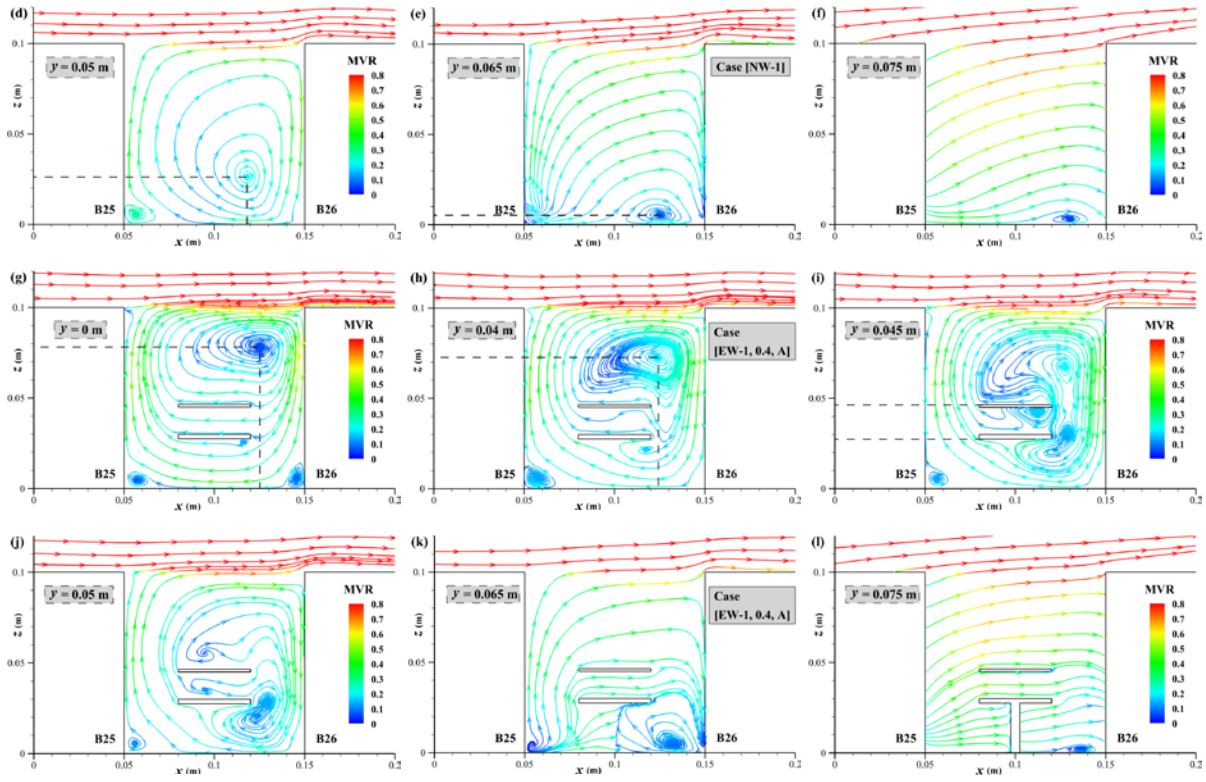

Fig. 6. 2D streamlines of mean flows at XZ planes for (a-f) Case [NW-1] and (g-l) Case [EW-1, 0.4, A].

3.3. Effect of street aspect ratios (*H/W*)

3.3.1. Mean wind velocity

Fig. 7 depicts MVR contours at the pedestrian level in Case [NW-1], Case [EW-1, 0.4, A], Case [NW-2], Case [EW-2, 0.4, A], Case [NW-3], and Case [EW-3, 0.4, A]. Referring to Zhang et al. [42] and Liu et al. [40], we defined three mean wind velocity ratio regions based on MVR values, namely low (MVR < 0.3), medium ($0.3 \leq MVR \leq 0.7$), and high (0.7 < MVR) mean wind velocity ratio regions. Obviously, the overall MVR value in the side street is generally greater than in the target street owing to the strong external flow. Comparing Case [EW-1, 0.4, A] with Case [NW-1] (see Fig. 7(a-b)), it is clear that the area of medium MVR regions (i.e., green zones) in the target canyon shrinks after adding the elevated walkway. Area ratios of low ($AR_{MVR<0.3}$) and medium ($AR_{0.3 \leq MVR \leq 0.7}$) MVR regions to the target street and area-averaged MVR values were calculated to quantify pedestrian-level mean wind environments in the target

street. As presented in Table 3, the area ratio of medium MVR regions to the target street drops from 38.42% to 19.51%. Furthermore, the area-averaged MVR value of the target street in Case [EW-1, 0.4, A] decreases by about 13.33%. Overall, concerning the unit-aspect-ratio urban street canyon, the elevated walkway has an adverse effect on the pedestrian-level mean wind environment of the target street.

Compared to cases with *H/W* =1, street canyon mean flows are attenuated drastically in Case [NW-2] and Case [EW-2, 0.4, A] (see Fig. 7(c-d)). Doubling building height from *H/W* =1 to 2 causes considerable blocking effects on canyon flows. The low MVR region dominates the entire target street. Table 3 shows that the area-averaged MVR values of the target street in Case [NW-2] and Case [EW-2, 0.4, A] are about 0.144 and 0.093, dropping by 43.53% and 57.92%, respectively. Moreover, the adverse impact of the elevated walkway on the pedestrian-level mean wind environment of the target street is remarkable, as the area-averaged MVR value in Case [EW-2, 0.4, A] is around 35.42% smaller than Case [NW-2].

Unlike doubling building height from *H/W* =1 to 2, heightening building height from *H/W* = 2 to 3 improves street canyon mean flows. As presented in Fig. 7(e-f), Case [NW-3] and Case [EW-3, 0.4, A] have enlarged medium MVR regions in the target street. Furthermore, as shown in Table 3, the area-averaged MVR values of the target street rise to ~0.170 and ~0.130 in Case [NW-3] and Case [EW-3, 0.4, A], respectively. The above result also indicates that adding an elevated walkway in Case [NW-3] decreases the area-averaged MVR value of the target street by ~23.53%. The improvement of pedestrian-level mean wind environments in cases with *H/W* = 3 can be attributed to enhanced channeling flows in two main streets. The area-averaged MVR value of main streets in Case [NW-3] increases by ~83.33% compared to Case [NW-2]. Likewise, Case [EW-3, 0.4, A] has a ~79.82% rise in the area-averaged MVR value of main streets to Case [EW-2, 0.4, A].

In summary, in terms of ideal urban street canyons with *H/W* = 1, 2, and 3, building an elevated walkway in the central road will lower the pedestrian-level mean wind velocity of the target street. When the building height increases, channeling flows at the entrance of main streets will be strengthened significantly due to the venturi effect. Meanwhile, the wind-blocking effect of buildings is enhanced. In this case, the target street's overall mean wind velocity at the pedestrian level declines first and then rises with *H/W*. Dai et al. [58] previously reported that the pollutant concentration displays a rising tendency when *H/W* is between 0.5 and 1.25 but a dropping trend when *H/W* increases from 1.25 to 2. Therefore, a turning value of *H/W* may exist in the three-row by seven-column urban street canyon model. The pedestrian-level mean wind environment will be worst in this turning case. Further studies are required to verify the above conclusion and identify the turning value of *H/W*.

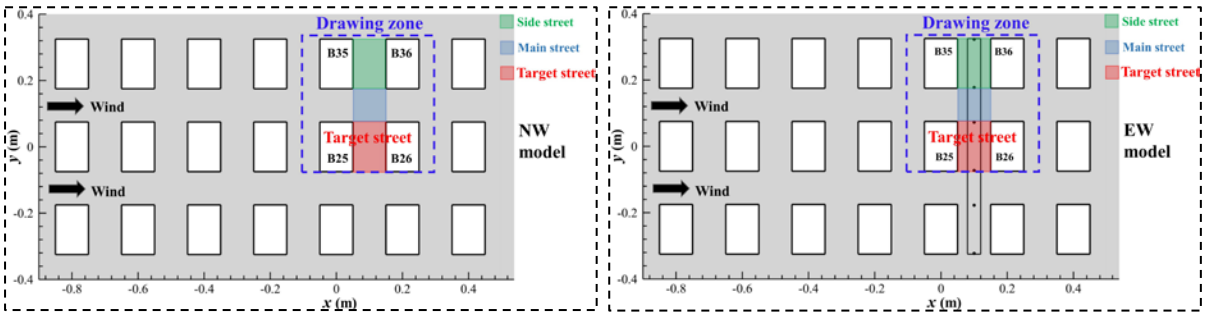

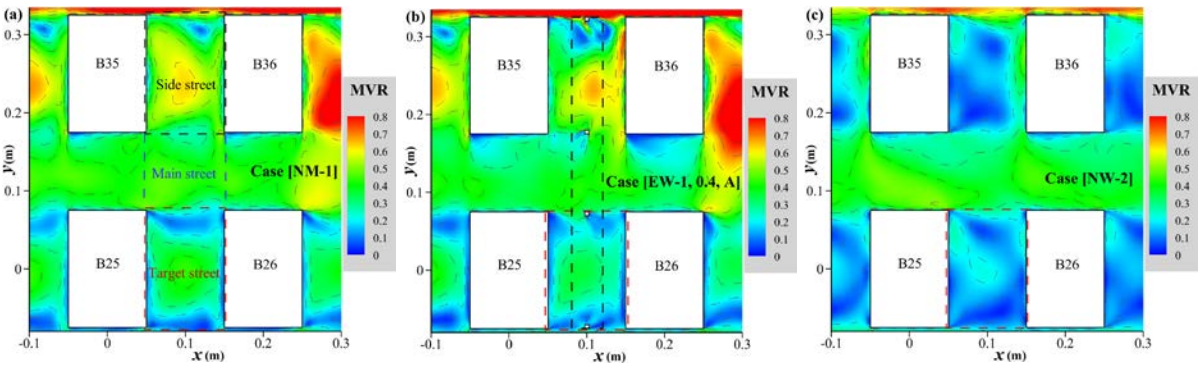

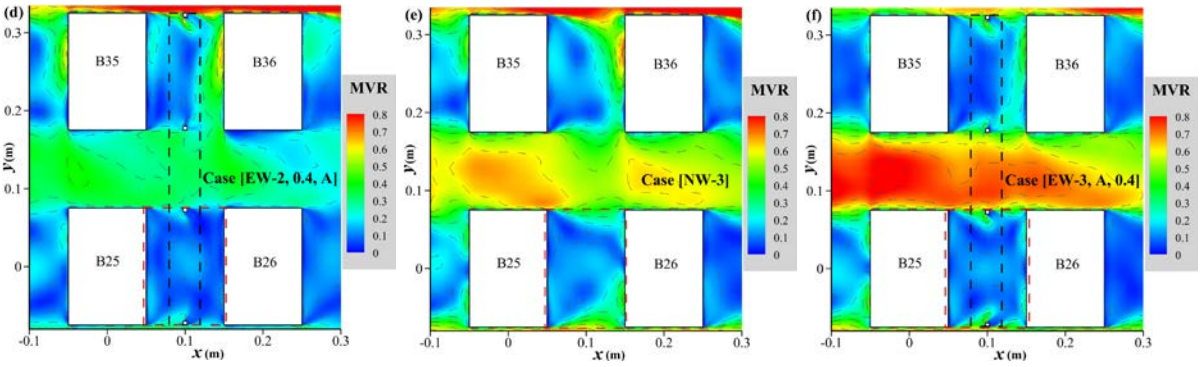

Fig. 7. Pedestrian-level mean wind velocity ratio (MVR) contours in cases with different street aspect ratios (H/W = 1, 2, 3). The target street is located between B25 and B26.

Table 3. Summary of area ratios of low ($AR_{MVR < 0.3}$) and medium ($AR_{0.3 \le MVR \le 0.7}$) MVR regions to the target street and area-averaged MVR values in the target street for cases with different street aspect ratios (H/W).

Type	Case name	H/W	$AR_{MVR < 0.3}$	$AR_{0.3 \le MVR \le 0.7}$	Area-weighted MVR
No-walkway	Case [NW-1]	1	61.58%	38.42%	0.255
	Case [NW-2]	2	100.00%	0	0.144
	Case [NW-3]	3	88.44%	11.56%	0.170
Elevated walkway	Case [EW-1, 0.4, A]	1	80.16%	19.51%	0.221
	Case [EW-2, 0.4, A]	2	99.67%	0	0.093
	Case [EW-3, 0.4, A]	3	94.69%	4.98%	0.130

3.3.2. Gust wind velocity

In terms of wind force, people generally perceive the gust and associated change rate most [8]. In other words, the gust wind velocity $\widehat{U}$ is a significant metric to assess the mechanical effect of wind on people. Melbourne [8] defined $\widehat{U}$ as $\overline{U} \times (1 + 3.5TI)$, where $\overline{U}$ is the mean wind velocity and TI is the turbulence intensity. According to this definition, the gust wind velocity characterizes the combined effects of mean wind velocity and turbulence intensity.

Similar to MVR, the gust wind velocity ratio (GVR) is prescribed as $\widehat{U}/\overline{U}_{2m}$. Three gust wind velocity regions are distinguished: low GVR region with GVR < 1.2, medium GVR region with $1.2 \leq \text{GVR} \leq 2$, and high GVR region with 2 < GVR. Additionally, this study defines areas with 2 < *TI* as high turbulence intensity regions.

Fig. 8 depicts distributions of the gust wind velocity ratio at the pedestrian level in Case [NW-1], Case [NW-2], Case [NW-3], Case [EW-1, 0.4, A], Case [EW-2, 0.4, A], and Case [EW-3, 0.4, A]. Area ratios of low GVR regions ($AR_{GVR < 1.2}$) and high *TI* regions ($AR_{2 < TI}$) to the target street and area-averaged GVR and *TI* values in the target street for these cases are summarized in Table 4. As is evident from Fig. 8(a-b), the low and medium GVR regions account for the entire target street in *H/W* = 1. In contrast to Case [NW-1], Case [EW-1, 0.4, A] has a significantly larger low GVR region. Specifically, according to Table 4, the area ratio of the low GVR region to the target street in Case [EW-1, 0.4, A] increases more than five times, changing from 3.93% to 22.33%. Consequently, the area-averaged GVR value of the target street in Case [EW-1, 0.4, A] decreases to 1.328, about 17.52% smaller than in Case [NW-1]. Table 4 also indicates that the high *TI* region and area-averaged *TI* value in Case [EW-1, 0.4, A] diminish due to the elevated walkway. This finding explains why the elevated walkway exhibits more significant effects on GVR than MVR.

Likewise, it is manifest from Fig. 8(c-d) that the walkway case has lower gust wind velocities than the corresponding no-walkway one in *H/W* = 2. As Table 4 displays, the area ratio of the low GVR region to the target street is approximately 60.90% in Case [NW-2], whereas the area ratio increases to about 97.30% in Case [EW-2, 0.4, A]. Therefore, the area-averaged GVR value of the target street in Case [EW-2, 0.4, A] dwindles to 0.909, about 22.24% smaller than in Case [NW-2]. Compared to Case [EW-1, 0.4, A] (see Fig. 8(b)), Case [EW-2, 0.4, A] experiences a drastic shrinkage in the medium GVR region, with the low GVR region dominating the target street. Consequently, Case [EW-2, 0.4, A] has a ~31.55% smaller area-

averaged GVR value than Case [EW-1, 0.4, A] in the target street. Significantly, amplitudes of change in GVR, caused by the elevated walkway and street aspect ratio, are smaller than in MVR. Such results can be attributed to *TI* showing opposite changes to MVR and GVR. As shown in Table 4, Case [EW-2, 0.4, A] has a larger high *TI* region and area-averaged *TI* value than Case [NW-2] and Case [EW-1, 0.4, A].

As illustrated in Fig. 8(e-f), although the low GVR region still occupies most of the target street in $H/W = 3$, its size diminishes compared to $H/W = 2$. Table 4 indicates that the area ratios of the low GVR region to the target street are approximately 59.99% and 75.41% in Case [NW-3] and Case [EW-3, 0.4, A], respectively. And the area-averaged GVR values of the target street are 1.145 and 1.054 in these two cases. It is plain that adding an elevated walkway to the ideal urban street with $H/W = 3$ increases the low GVR region size by ~25.70% and decreases the area-weighted GVR value by ~7.95%. Additionally, the variation in the overall gust wind velocity is insignificant between Case [NW-2] and Case [NW-3] but more significant between Case [EW-2, 0.4, A] and Case [EW-3, 0.4, A]. In contrast to Case [EW-2, 0.4, A], Case [EW-3, 0.4, A] obtains a ~22.50% decrease in the low GVR region and a ~15.95% increase in the area-averaged GVR value of the target street. Besides, *TI* still exhibits different variation trends from MVR and GVR, as shown in Table 4. Specifically, Case [EW-3, 0.4, A] has about 49.47% bigger high *TI* region and 22.00% greater area-averaged *TI* value than Case [NW-3]; Case [EW-3, 0.4, A] has approximately 12.92% smaller high *TI* region and 19.58% lower area-averaged *TI* value than Case [EW-2, 0.4, A].

In summary, the above results demonstrate that adding the elevated walkway to ideal urban streets with $H/W = 1$, 2, and 3 will lower the target street's overall pedestrian-level gust wind velocity and augment the size of the low gust wind velocity region. Regarding elevated walkway cases, the target street's overall pedestrian-level gust wind velocity is reduced with H/W rising from 1 to 2 but improved when H/W increases to 3. As the gust and mean wind

velocities share similar variation trends with *H/W*, it can be concluded that the mean wind velocity contributes more to the gust wind velocity than the turbulence intensity.

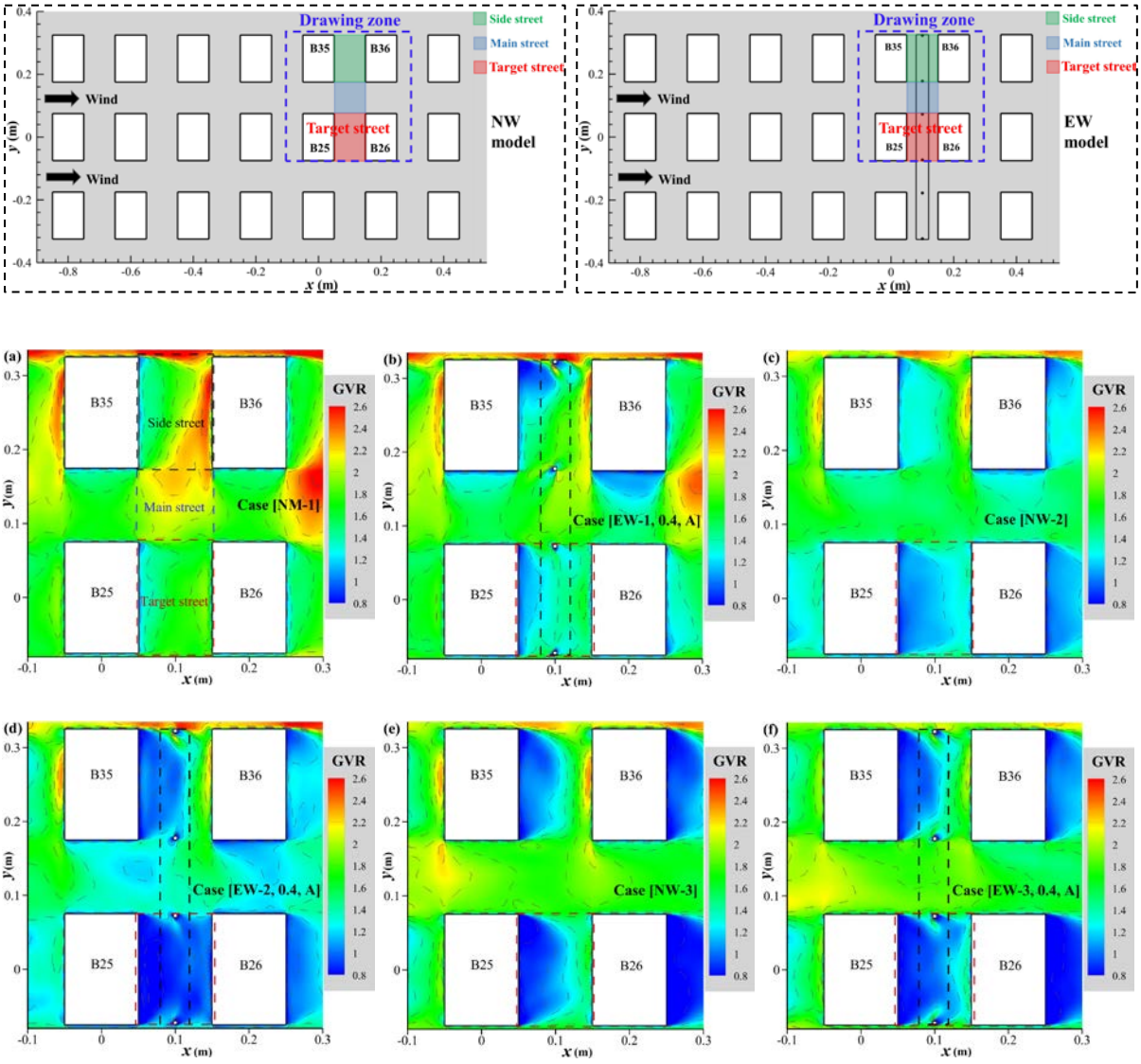

Fig. 8. Contours of the gust wind velocity ratio (GVR) at the pedestrian level in cases with different street aspect ratios (*H/W* = 1, 2, 3).

Table 4. Area ratios of low GVR regions ($AR_{GVR < 1.2}$) and high *TI* regions ($AR_{2 < TI}$) to the target street and area-averaged GVR and *TI* values in the target street for cases with different street aspect ratios.

Type	Case name	*H/W*	$AR_{GVR < 1.2}$	$AR_{2 < TI}$	Area-weighted GVR	Area-weighted *TI*

No-walkway	Case [NW-1]	1	3.93%	33.81%	1.610	1.920
	Case [NW-2]	2	60.90%	49.52%	1.169	2.536
	Case [NW-3]	3	59.99%	41.56%	1.145	2.077
Elevated walkway	Case [EW-1, 0.4, A]	1	22.33%	26.65%	1.328	1.735
	Case [EW-2, 0.4, A]	2	97.30%	71.34%	0.909	3.151
	Case [EW-3, 0.4, A]	3	75.41%	62.12%	1.054	2.534

3.4. Effect of elevated walkway widths (W_{ew}/W)

3.4.1. 2D mean flow regime

This section examines pedestrian-level wind environments in three walkway widths (W_{ew}/W = 0.2, 0.4, and 0.6). As depicted in Fig. 9(a-f), even though the walkway narrows to one in five of the street width, it still affects the flow regime at XZ-planes. Case [EW-1, 0.2, A] resembles Case [EW-1, 0.4, A] in the evolution of 2D XZ-plane streamlines alone spanwise street. When the walkway widens to three in five of the street width (see Fig. 9(g-l)), its partition effect on the canyon flow becomes more significant. The walkway cover acts as a new ground for the upper canyon, preserving the elevated vortex center from rapid distortion (e.g., from y = 0 to 0.05 m). Meanwhile, another clearly defined vortex center forms below the walkway floor. At y = 0.05 m, the mean flow is weak and complicated in the walkway interior, with small vortices existing. The distributions of pedestrian-level mean wind velocity and gust wind velocity will be discussed in detail below.

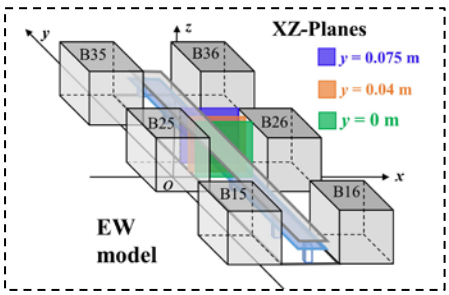

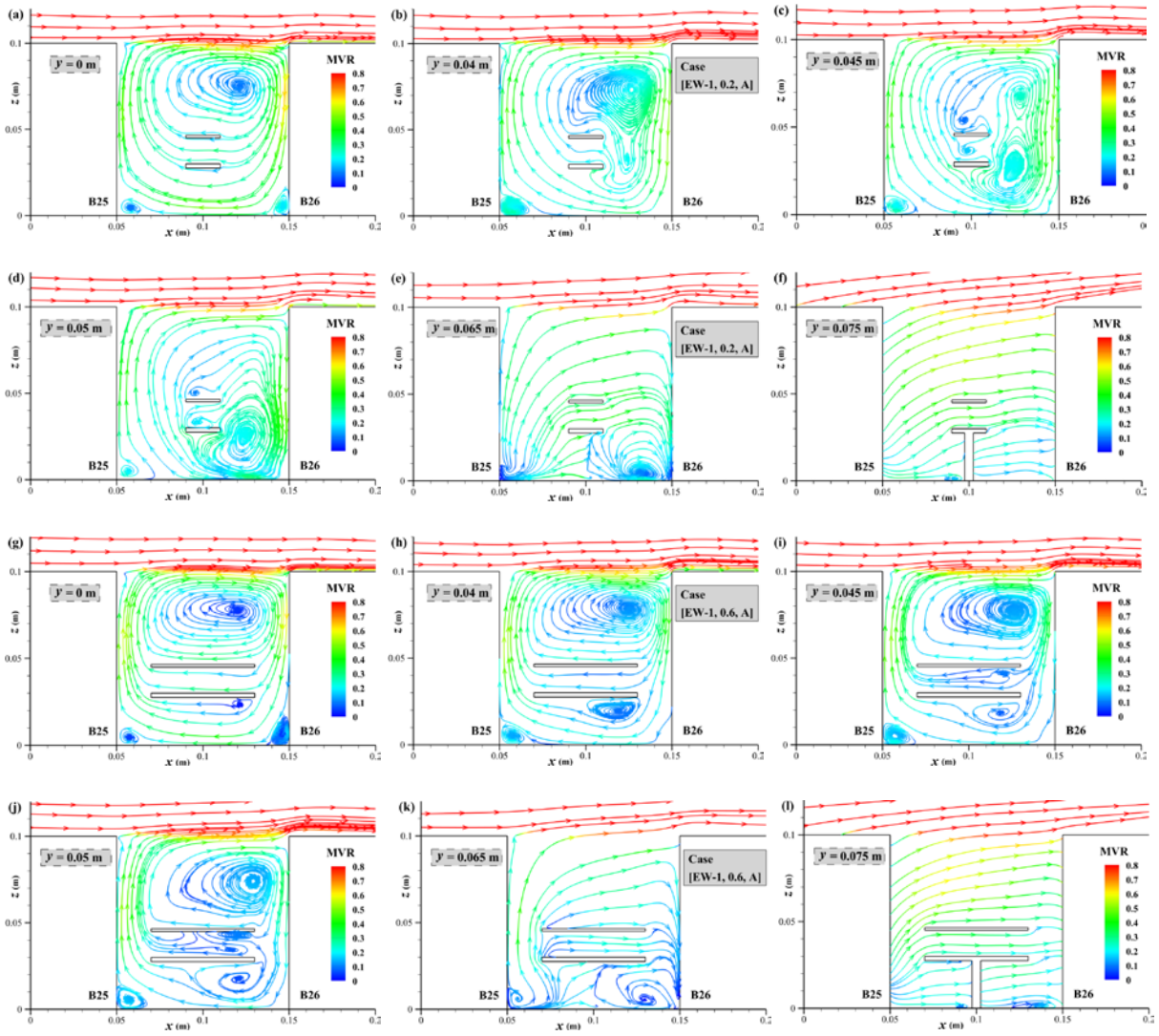

Fig. 9. 2D streamlines of mean flows at XZ planes for (a-f) Case [EW-1, 0.2, A] and (g-l) Case [EW-1, 0.6, A].

3.4.2. Mean wind velocity

Fig. 10(a-b) presents distributions of pedestrian-level MVR in Case [EW-1, 0.2, A] and Case [EW-1, 0.6, A]. Similar to Case [EW-1, 0.4, A] (see Fig. 7(b)), a relatively small medium MVR region exists in the middle of the target street, surrounded by a large low MVR region. Area ratios of the medium MVR region to the target street and average-weighted MVR values in the target street are shown in Table 5. It is evident from the figure and table that the medium MVR region shrinks considerably as the elevated walkway widens. The area-averaged MVR values of the target street in Case [EW-1, 0.2, A], Case [EW-1, 0.4, A], and [EW-1, 0.6, A] are

about 0.252, 0.221, and 0.186, respectively. The above results indicate that the overall MVR value of the target street at the pedestrian level shows a declining trend with increasing elevated walkway width. This finding can be explained by the downward flow along the windward wall weakening with the rise of the walkway width.

3.4.3. Gust wind velocity

Contours of pedestrian-level GVR in Case [EW-1, 0.2, A] and Case [EW-1, 0.6, A] are depicted in Fig. 10(c-d). In contrast to Fig. 8(b), it is clear that the size of low GVR regions grows significantly with the elevated walkway width. Table 5 enumerates area ratios of low GVR and high *TI* regions to the target street and average-weighted GVR and *TI* values of the target street under three walkway widths. It can be found that the area ratio of high *I* regions and the area-averaged *I* value show a rising trend with the walkway width, which is opposite to MVR. Regarding GVR, the low GVR region in the target street increases by about 170.67% from $W_{ew}/W = 0.2$ to 0.4 and 134.53% from $W_{ew}/W = 0.4$ to 0.6. Furthermore, the area-averaged GVR values of the target street in these three cases are approximately 1.454, 1.328, and 1.188, indicating a slightly decreasing trend with the increase of the walkway width. The variation rule also applies to main and side streets.

In conclusion, when the elevated walkway broadens, the target street's pedestrian-level mean and gust wind velocities decline while the turbulence intensity presents an increasing tendency. The walkway's extension strengthens the blocking effect on the canyon flow transporting downward, causing weakened pedestrian-level mean and gust wind environments.

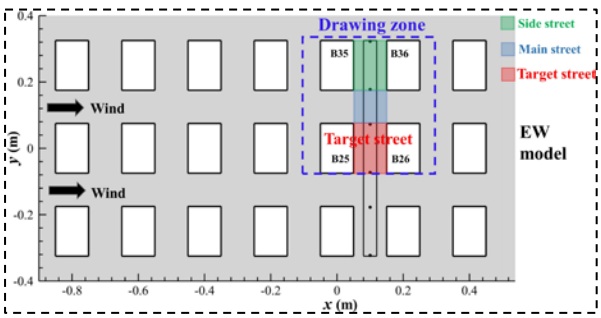

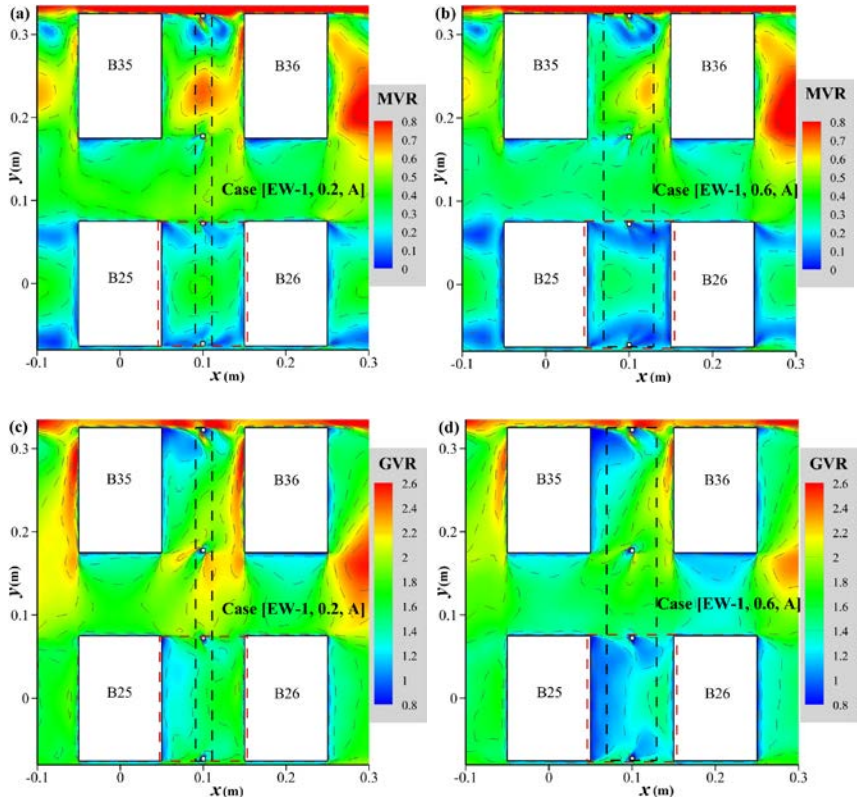

Fig. 10. Contours of (a-b) the pedestrian-level mean wind velocity ratio (MVR) and (c-d) gust wind velocity ratio (GVR) in Case [EW-1, 0.2, A] and Case [EW-1, 0.6, A].

Table 5. Summary of area ratios of medium MVR regions ($AR_{0.3 \le MVR \le 0.7}$), low GVR regions ($AR_{GVR < 1.2}$), and high *TI* regions ($AR_{2 < TI}$) to the target street and area-averaged MVR, GVR, and *TI* values of the target street under three walkway widths (W_{ew}/W).

Case name	W_{ew}/W	$AR_{0.3 \le MVR \le 0.7}$	$AR_{GVR < 1.2}$	$AR_{2 < TI}$	Area-weighted MVR	Area-weighted GVR	Area-weighted *TI*
Case [EW-1, 0.2, A]	0.2	33.79%	8.25%	23.14%	0.252	1.454	1.627
Case [EW-1, 0.4, A]	0.4	19.51%	22.33%	26.65%	0.221	1.328	1.735
Case [EW-1, 0.6, A]	0.6	7.79%	52.37%	36.74%	0.186	1.188	1.971

3.5. Effect of walkway sidewall types (Type A, B, C)

3.5.1. Mean wind velocity

493 This section compares the pedestrian-level wind environment under open (Type A), semi-
494 hermetic (Type B), and hermetic sidewall (Type C) conditions. Fig. 11(a-b) depicts
495 distributions of MVR at the pedestrian level in Case [EW-1, 0.4, B] and Case [EW-1, 0.4, C].
496 In contrast to the open condition (see Fig. 7(b)), it can be observed that the medium MVR
497 region of the target street is expanded after adding semi-hermetic or hermetic sidewalls. As
498 Table 6 shows, the area ratios of the medium MVR region to the target street in Case [EW-1,
499 0.4, B] and Case [EW-1, 0.4, C] are about 31.28% and 20.59%, which are around 60.33% and
500 5.54% larger than Case [EW-1, 0.4, A], respectively. Moreover, Case [EW-1, 0.4, B] and Case
501 [EW-1, 0.4, C] have about 8.14% and 4.07% greater area-averaged MVR values of the target
502 street than Case [EW-1, 0.4, A]. Results demonstrate that adding semi-hermetic or hermetic
503 sidewalls improves the pedestrian-level mean wind environment in the target street to some
504 extent. The pedestrian-level wind velocity of the target street depends upon entrained flow from
505 the roof and main streets. Due to the walkway sidewall, downdrafts are strengthened near the
506 windward sides of the main streets and building B26. And this enhanced downdraft can increase
507 area-averaged MVR values in main streets under semi-hermetic and hermetic sidewall
508 conditions.

509 3.5.2. Gust wind velocity

510 The pedestrian-level GVR contours in Case [EW-1, 0.4, B] and Case [EW-1, 0.4, C] are
511 illustrated in Fig. 11(c-d). It is manifest that Case [EW-1, 0.4, B] and Case [EW-1, 0.4, C] have
512 larger “green” regions (GVR > 1.4) than Case [EW-1, 0.4, A] (see Fig. 8(b)). But the difference
513 in the size of low GVR regions is insignificant under three sidewall conditions. Table 6 presents
514 that the area ratios of the low GVR region to the target street are 21.77% and 20.52% in Case
515 [EW-1, 0.4, B] and Case [EW-1, 0.4, C], which are about 2.51% and 8.11% lower than Case
516 [EW-1, 0.4, A]. Likewise, the increase in the area-averaged GVR value of the target street is
517 minor under semi-hermetic and hermetic sidewall conditions. Compared to Case [EW-1, 0.4,

A], the area-averaged GVR values of the target street in Case [EW-1, 0.4, B] and Case [EW-1, 0.4, C] only increase by 0.53% and 2.11%, respectively. Considering *TI*, as is displayed in Table 6 that both Case [EW-1, 0.4, B] and Case [EW-1, 0.4, C] have smaller high *TI* regions than Case [EW-1, 0.4, A]. Furthermore, the area-averaged *TI* values of the target street in Case [EW-1, 0.4, B] and Case [EW-1, 0.4, C] are about 1.657 and 1.631, which are 4.50% and 5.99% lower than Case [EW-1, 0.4, A]. Therefore, adding semi-hermetic or hermetic sidewalls to the elevated walkway weakens the pedestrian-level turbulence intensity in the target street by a small margin. Undoubtedly, the decreased turbulence intensity counteracts the increased mean wind velocity, causing an insignificant change in the gust wind velocity. In conclusion, adding semi-hermetic or hermetic sidewalls to the elevated walkway enhances the pedestrian-level gust wind velocity in the target street. Nevertheless, the overall effects of sidewalls on the gust wind environment are insignificant.

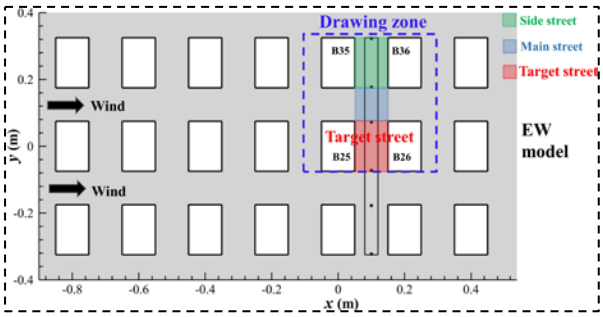

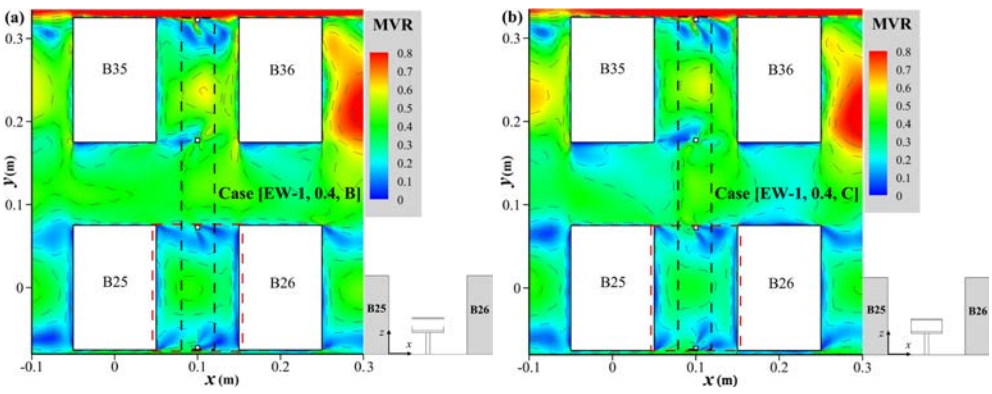

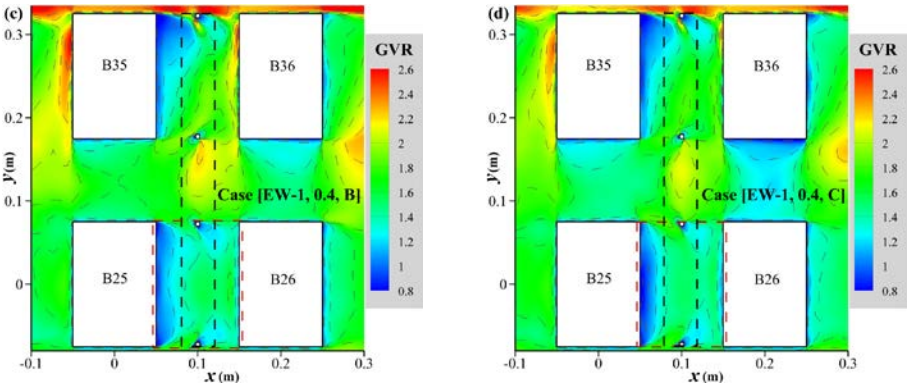

Fig. 11. Contours of (a-b) the pedestrian-level mean wind velocity ratio (MVR) and (c-d) gust wind velocity ratio (GVR) in Case [EW-1, 0.4, B] and Case [EW-1, 0.4, C].

Table 6. Summary of area ratios of medium MVR regions ($AR_{0.3 \le MVR \le 0.7}$), low GVR regions ($AR_{GVR < 1.2}$), and high *TI* regions ($AR_{2 < TI}$) to the target street and area-averaged MVR, GVR, and *TI* values of the target street under three sidewall types.

Case name	Sidewall type	$AR_{0.3 \le MVR \le 0.7}$	$AR_{GVR < 1.2}$	$AR_{2 < TI}$	Area-weighted MVR	Area-weighted GVR	Area-weighted *TI*
Case [EW-1, 0.4, A]	open	19.51%	22.33%	26.65%	0.221	1.328	1.735
Case [EW-1, 0.4, B]	semi-hermetic	31.28%	21.77%	23.29%	0.239	1.335	1.657
Case [EW-1, 0.6, C]	hermetic	20.59%	20.52%	22.30%	0.230	1.356	1.631

4. Conclusions

4.1. Summary

This study investigated the effects of the elevated walkway, street aspect ratio, walkway width, and sidewall type on the pedestrian-level wind environment in ideal urban street canyons under perpendicular wind direction. A series of large eddy simulations were performed to predict the mean and gust wind velocity fields under different street aspect ratios and walkway designs. Given that low to medium mean and gust wind velocity regions (i.e., MVR $\le$ 0.7 and GVR $\le$ 2) dominate the target street for all cases, this study prescribes that the higher the mean

and gust wind velocities, the better the pedestrian-level mean and gust wind environments. The main findings are summarized as follows:

(1) The elevated walkway adversely affects the target street's pedestrian-level wind environment, as the overall mean and gust wind velocities are attenuated after adding an elevated walkway. The maximum decline rates can reach 35.42% and 22.24% in the area-averaged MVR and GVR values, respectively.

(2) The effects of street aspect ratio (*H/W*) on the target street' pedestrian-level wind environment are non-monotonic. The overall mean and gust wind velocities at the pedestrian level decrease as *H/W* varies from 1 to 2 but increase when *H/W* continues rising to 3. There might be a turning value of *H/W*, where the mean and gust wind velocities reach the minimum and the wind environment is worst.

(3) When the elevated walkway widens, the pedestrian-level mean and gust wind flows are decelerated in the target street. Thus, the pedestrian-level wind environment worsens with increased walkway width. Extremely wide elevated walkways should be avoided.

(4) Compared to the open condition, the target street's overall mean and gust wind velocities slightly improve at the pedestrian level under semi-hermetic and hermetic sidewall conditions. But the effect of sidewall types on the pedestrian-level wind environment is insignificant.

This study fills the research gap on the impacts of elevated walkway design parameters and street aspect ratio on pedestrian-level mean and gust wind environments. The findings can be helpful references for urban planners and constructors in designing elevated walkway frameworks.

4.2. Limitations and future work

Despite these contributions, this study was conducted with some limitations. First, this study only considers the perpendicular wind direction, which is usually most unfavorable for canyon flows. However, the approaching wind direction generally affects the pedestrian-level wind environment inside the street. Thus, the results may differ under parallel and oblique wind directions. Further investigations on more typical wind directions are needed. Second, our elevated walkway model is as long as the street and parallel to the street orientation. The conclusions based on this parallel walkway design may not apply to other walkway types. For instance, another typical walkway spans the road and is usually much shorter. Such a perpendicular walkway design should be less intrusive to the canyon flow than the parallel one. Third, the parametric study on pedestrian-level wind environment is limited to three parameters: street aspect ratio, walkway width, and sidewall type. Urban street canyons and elevated walkways have various forms in the actual world. Other geometric parameters such as the street layout, walkway height and position, height and interval distance of supporting pillars, and cover configuration are worth investigating. Last, all CFD simulations were performed under an isothermal condition, ignoring thermal effects. Further study on non-isothermal conditions is required.

Although this study obtained some significant results on the wind environment, it is the beginning of further research on elevated walkways. The elevated walkway with a cover can provide shade for pedestrians, so its impact on pedestrian thermal comfort is of research significance. Future work will focus on other influential parameters and how the elevated walkway influences pedestrian thermal comfort.

CRediT authorship contribution statement

Lan Chen: Conceptualization, Methodology, Software, Validation, Formal analysis, Investigation, Writing - Original Draft, Writing - Review & Editing, Visualization. **Cheuk**

Ming Mak: Conceptualization, Resources, Writing - Review & Editing, Supervision, Funding acquisition. **Jian Hang:** Conceptualization, Resources, Funding acquisition. **Yuwei Dai:** Methodology, Validation. **Jianlei Niu:** Resources, Funding acquisition. **Kam Tim Tse:** Resources, Funding acquisition.

Declaration of competing interests

The authors declare that they have no known competing financial interests or personal relationships that could have appeared to influence the work reported in this paper.

Acknowledgments

This work was supported by the Research Grants Council of the Hong Kong Special Administrative Region, China (Project No. T22-504/21-R), the National Natural Science Foundation of China (Project No. 42175095), and a PhD studentship funded by The Hong Kong Polytechnic University. CFD simulations of this work were conducted on the Tianhe II supercomputer at the National Supercomputer Center in Guangzhou, China.

References

[1] T. Bentham, R. Britter, Spatially averaged flow within obstacle arrays, Atmospheric Environment 37(15) (2003) 2037-2043, https://doi.org/10.1016/s1352-2310(03)00123-7.

[2] E. Ng, V. Cheng, Urban human thermal comfort in hot and humid Hong Kong, Energy and Buildings 55 (2012) 51-65, https://doi.org/10.1016/j.enbuild.2011.09.025.

[3] E. Ng, Policies and technical guidelines for urban planning of high-density cities - air ventilation assessment (AVA) of Hong Kong, Building and Environment 44(7) (2009) 1478-1488, https://doi.org/10.1016/j.buildenv.2008.06.013.

[4] J. Hang, Y. Li, M. Sandberg, *et al.*, The influence of building height variability on pollutant dispersion and pedestrian ventilation in idealized high-rise urban areas, Building and Environment 56 (2012) 346-360, https://doi.org/10.1016/j.buildenv.2012.03.023.

[5] J. Hang, Z. Luo, X. Wang, *et al.*, The influence of street layouts and viaduct settings on daily carbon monoxide exposure and intake fraction in idealized urban canyons, Environmental Pollution 220(Pt A) (2017) 72-86, https://doi.org/10.1016/j.envpol.2016.09.024.

[6] B. Blocken, W.D. Janssen, T. van Hooff, CFD simulation for pedestrian wind comfort and wind safety in urban areas: General decision framework and case study for the Eindhoven University campus, Environmental Modelling & Software 30 (2012) 15-34, https://doi.org/10.1016/j.envsoft.2011.11.009.

[7] T. van Druenen, T. van Hooff, H. Montazeri, *et al.*, CFD evaluation of building geometry modifications to reduce pedestrian-level wind speed, Building and Environment 163 (2019), https://doi.org/10.1016/j.buildenv.2019.106293.

[8] W.H. Melbourne, Criteria for environmental wind conditions, Journal of Wind Engineering and Industrial Aerodynamics 3(2-3) (1978) 241-249, https://doi.org/10.1016/0167-6105(78)90013-2.

[9] M.J. Soligo, P.A. Irwin, C.J. Williams, *et al.*, A comprehensive assessment of pedestrian comfort including thermal effects, Journal of Wind Engineering and Industrial Aerodynamics 77-8 (1998) 753-766, https://doi.org/10.1016/S0167-6105(98)00189-5.

[10] NEN, Wind comfort and wind danger in the built environment, Netherlands Normalisation Institute, NEN8100 (in Dutch), 2006.

[11] R. Buccolieri, M. Sandberg, S. Di Sabatino, City breathability and its link to pollutant concentration distribution within urban-like geometries, Atmospheric Environment 44(15) (2010) 1894-1903, https://doi.org/10.1016/j.atmosenv.2010.02.022.

[12] L. Peng, J.-P. Liu, Y. Wang, *et al.*, Wind weakening in a dense high-rise city due to over nearly five decades of urbanization, Building and Environment 138 (2018) 207-220, https://doi.org/10.1016/j.buildenv.2018.04.037.

[13] L. Tsichritzis, M. Nikolopoulou, The effect of building height and façade area ratio on pedestrian wind comfort of London, Journal of Wind Engineering and Industrial Aerodynamics 191 (2019) 63-75, https://doi.org/10.1016/j.jweia.2019.05.021.

[14] W. Wang, T. Yang, Y. Li, *et al.*, Identification of pedestrian-level ventilation corridors in downtown Beijing using large-eddy simulations, Building and Environment 182 (2020), https://doi.org/10.1016/j.buildenv.2020.107169.

[15] J. Jacob, P. Sagaut, Wind comfort assessment by means of large eddy simulation with lattice Boltzmann method in full scale city area, Building and Environment 139 (2018) 110-124, https://doi.org/10.1016/j.buildenv.2018.05.015.

[16] Y.-H. Juan, A.-S. Yang, C.-Y. Wen, *et al.*, Optimization procedures for enhancement of city breathability using arcade design in a realistic high-rise urban area, Building and Environment 121 (2017) 247-261, https://doi.org/10.1016/j.buildenv.2017.05.035.

[17] T. Ma, T. Chen, Outdoor ventilation evaluation and optimization based on spatial morphology analysis in Macau, Urban Climate 46 (2022), https://doi.org/10.1016/j.uclim.2022.101335.

[18] A. Abd Razak, A. Hagishima, N. Ikegaya, *et al.*, Analysis of airflow over building arrays for assessment of urban wind environment, Building and Environment 59 (2013) 56-65, https://doi.org/10.1016/j.buildenv.2012.08.007.

[19] G. Chen, X. Yang, H. Yang, *et al.*, The influence of aspect ratios and solar heating on flow and ventilation in 2D street canyons by scaled outdoor experiments, Building and Environment 185 (2020), https://doi.org/10.1016/j.buildenv.2020.107159.

[20] L. Chen, J. Hang, M. Sandberg, *et al.*, The impacts of building height variations and building packing densities on flow adjustment and city breathability in idealized urban models, Building and Environment 118 (2017) 344-361, https://doi.org/10.1016/j.buildenv.2017.03.042.

[21] L.W. Chew, L.K. Norford, Pedestrian-level wind speed enhancement with void decks in three-dimensional urban street canyons, Building and Environment 155 (2019) 399-407, https://doi.org/10.1016/j.buildenv.2019.03.058.

[22] L. Chen, C.M. Mak, Numerical evaluation of pedestrian-level wind comfort around “lift-up” buildings with various unconventional configurations, Building and Environment 188 (2021), https://doi.org/10.1016/j.buildenv.2020.107429.

[23] S.-J. Mei, J.-T. Hu, D. Liu, *et al.*, Wind driven natural ventilation in the idealized building block arrays with multiple urban morphologies and unique package building density, Energy and Buildings 155 (2017) 324-338, https://doi.org/10.1016/j.enbuild.2017.09.019.

673 [24] E. Ng, C. Yuan, L. Chen, *et al.*, Improving the wind environment in high-density cities by
674 understanding urban morphology and surface roughness: A study in Hong Kong, Landscape and Urban
675 Planning 101(1) (2011) 59-74, https://doi.org/10.1016/j.landurbplan.2011.01.004.
676 [25] J. Hang, Y. Li, M. Sandberg, Experimental and numerical studies of flows through and within high-
677 rise building arrays and their link to ventilation strategy, Journal of Wind Engineering and Industrial
678 Aerodynamics 99(10) (2011) 1036-1055, https://doi.org/10.1016/j.jweia.2011.07.004.
679 [26] D. Cui, G. Hu, Z. Ai, *et al.*, Particle image velocimetry measurement and CFD simulation of
680 pedestrian level wind environment around U-type street canyon, Building and Environment 154 (2019)
681 239-251, https://doi.org/10.1016/j.buildenv.2019.03.025.
682 [27] L. He, J. Hang, X. Wang, *et al.*, Numerical investigations of flow and passive pollutant exposure
683 in high-rise deep street canyons with various street aspect ratios and viaduct settings, Science of The
684 Total Environment 584-585 (2017) 189-206, https://doi.org/10.1016/j.scitotenv.2017.01.138.
685 [28] D. Cui, X. Li, Y. Du, *et al.*, Effects of envelope features on wind flow and pollutant exposure in
686 street canyons, Building and Environment 176 (2020), https://doi.org/10.1016/j.buildenv.2020.106862.
687 [29] Y. Zhang, C. Ou, L. Chen, *et al.*, Numerical studies of passive and reactive pollutant dispersion in
688 high-density urban models with various building densities and height variations, Building and
689 Environment 177 (2020), https://doi.org/10.1016/j.buildenv.2020.106916.
690 [30] J. Zhong, J. Liu, Y. Xu, *et al.*, Pedestrian-level gust wind flow and comfort around a building array–
691 Influencing assessment on the pocket park, Sustainable Cities and Society 83 (2022),
692 https://doi.org/10.1016/j.scs.2022.103953.
693 [31] C. Sha, X. Wang, Y. Lin, *et al.*, The impact of urban open space and 'lift-up' building design on
694 building intake fraction and daily pollutant exposure in idealized urban models, Science of the Total
695 Environment 633 (2018) 1314-1328, https://doi.org/10.1016/j.scitotenv.2018.03.194.
696 [32] P. Xie, J. Yang, H. Wang, *et al.*, A New method of simulating urban ventilation corridors using
697 circuit theory, Sustainable Cities and Society 59 (2020), https://doi.org/10.1016/j.scs.2020.102162.
698 [33] Y. He, Z. Liu, E. Ng, Parametrization of irregularity of urban morphologies for designing better
699 pedestrian wind environment in high-density cities – A wind tunnel study, Building and Environment
700 226 (2022), https://doi.org/10.1016/j.buildenv.2022.109692.

[34] X. Liu, B. Huang, R. Li, *et al.*, Wind environment assessment and planning of urban natural ventilation corridors using GIS: Shenzhen as a case study, Urban Climate 42 (2022), https://doi.org/10.1016/j.uclim.2022.101091.

[35] Z. Liu, Z. Yu, X. Chen, *et al.*, An investigation on external airflow around low-rise building with various roof types: PIV measurements and LES simulations, Building and Environment 169 (2020), https://doi.org/10.1016/j.buildenv.2019.106583.

[36] X.L. Zhang, A.U. Weerasuriya, B. Lu, *et al.*, Pedestrian-level wind environment near a super-tall building with unconventional configurations in a regular urban area, Building Simulation 13(2) (2020) 439-456, https://doi.org/10.1007/s12273-019-0588-3.

[37] X.Y. Zhang, A.U. Weerasuriya, X.L. Zhang, *et al.*, Pedestrian wind comfort near a super-tall building with various configurations in an urban-like setting, Building Simulation (2020) 1-24, https://doi.org/10.1007/s12273-020-0658-6.

[38] X. Xu, Q. Yang, A. Yoshida, *et al.*, Characteristics of pedestrian-level wind around super-tall buildings with various configurations, Journal of Wind Engineering and Industrial Aerodynamics 166 (2017) 61-73, https://doi.org/10.1016/j.jweia.2017.03.013.

[39] C.Y. Wen, Y.H. Juan, A.-S. Yang, Enhancement of city breathability with half open spaces in ideal urban street canyons, Building and Environment 112 (2017) 322-336, https://doi.org/10.1016/j.buildenv.2016.11.048.

[40] J. Liu, X. Zhang, J. Niu, *et al.*, Pedestrian-level wind and gust around buildings with a ‘lift-up’ design: Assessment of influence from surrounding buildings by adopting LES, Building Simulation 12(6) (2019) 1107-1118, https://doi.org/10.1007/s12273-019-0541-5.

[41] Y. Du, C.M. Mak, Y. Li, Application of a multi-variable optimization method to determine lift-up design for optimum wind comfort, Building and Environment 131 (2018) 242-254, https://doi.org/10.1016/j.buildenv.2018.01.012.

[42] X. Zhang, K.T. Tse, A.U. Weerasuriya, *et al.*, Evaluation of pedestrian wind comfort near 'lift-up' buildings with different aspect ratios and central core modifications, Building and Environment 124 (2017) 245-257, https://doi.org/10.1016/j.buildenv.2017.08.012.

728 [43] X. Zheng, H. Montazeri, B. Blocken, CFD simulations of wind flow and mean surface pressure for
729 buildings with balconies: Comparison of RANS and LES, Building and Environment 173 (2020),
730 https://doi.org/10.1016/j.buildenv.2020.106747.
731 [44] M. Llaguno-Munitxa, E. Bou-Zeid, M. Hultmark, The influence of building geometry on street
732 canyon air flow: Validation of large eddy simulations against wind tunnel experiments, Journal of Wind
733 Engineering and Industrial Aerodynamics 165 (2017) 115-130,
734 https://doi.org/10.1016/j.jweia.2017.03.007.
735 [45] D. Cui, X. Li, J. Liu, *et al.*, Effects of building layouts and envelope features on wind flow and
736 pollutant exposure in height-asymmetric street canyons, Building and Environment 205 (2021),
737 https://doi.org/10.1016/j.buildenv.2021.108177.
738 [46] Y. Li, L. Chen, Study on the influence of voids on high-rise building on the wind environment,
739 Building Simulation 13(2) (2019) 419-438, https://doi.org/10.1007/s12273-019-0584-7.
740 [47] E.A. King, E.P. Bourdeau, X.Y.K. Zheng, *et al.*, A combined assessment of air and noise pollution
741 on the High Line, New York City, Transportation Research Part D: Transport and Environment 42 (2016)
742 91-103, https://doi.org/10.1016/j.trd.2015.11.003.
743 [48] H. Wang, P. Brimblecombe, K. Ngan, Particulate matter inside and around elevated walkways,
744 Science of The Total Environment 699 (2020) 134256, https://doi.org/10.1016/j.scitotenv.2019.134256.
745 [49] G. Duan, P. Brimblecombe, Y.L. Chu, *et al.*, Turbulent flow and dispersion inside and around
746 elevated walkways, Building and Environment 173 (2020),
747 https://doi.org/10.1016/j.buildenv.2020.106711.
748 [50] Footbridges and Subways of Hong Kong, Highways Department, Hong Kong, 2022.
749 https://www.hyd.gov.hk/en/information_corner/hyd_factsheets/doc/e_Footbridges_and_Subways.pdf.
750 [51] K.A. Robertson, Pedestrian skywalks in Calgary, Canada: : A comparison with US downtown
751 systems, Cities 4(3) (1987) 207-214, https://doi.org/10.1016/0264-2751(87)90029-1.
752 [52] F. Yang, F. Qian, W. Zhao, Towards a Climate-Responsive Vertical Pedestrian System: An
753 Empirical Study on an Elevated Walkway in Shanghai China, Sustainability 8(8) (2016),
754 https://doi.org/10.3390/su8080744.

[53] Proposed Pedestrian Footbridge System in Mong Kok Major Works Project Management Office, Highways Department, Hong Kong, 2017. https://www.hyd.gov.hk/en/our_projects/road_projects/mkfb/Local_Consultation_Paper_(Eng).pdf.

[54] B. Blocken, Computational Fluid Dynamics for urban physics: Importance, scales, possibilities, limitations and ten tips and tricks towards accurate and reliable simulations, Building and Environment 91 (2015) 219-245, https://doi.org/10.1016/j.buildenv.2015.02.015.

[55] Y. Toparlar, B. Blocken, B. Maiheu, *et al.*, A review on the CFD analysis of urban microclimate, Renewable and Sustainable Energy Reviews 80 (2017) 1613-1640, https://doi.org/10.1016/j.rser.2017.05.248.

[56] J. Zhong, J. Liu, Y. Zhao, *et al.*, Recent advances in modeling turbulent wind flow at pedestrian-level in the built environment, Architectural Intelligence 1(1) (2022) 5, https://doi.org/10.1007/s44223-022-00008-7.

[57] J. Liu, J. Niu, Y. Du, *et al.*, LES for pedestrian level wind around an idealized building array—Assessment of sensitivity to influencing parameters, Sustainable Cities and Society 44 (2019) 406-415, https://doi.org/10.1016/j.scs.2018.10.034.

[58] Y. Dai, C.M. Mak, Z. Ai, *et al.*, Evaluation of computational and physical parameters influencing CFD simulations of pollutant dispersion in building arrays, Building and Environment 137 (2018) 90-107, https://doi.org/10.1016/j.buildenv.2018.04.005.

[59] Z.T. Ai, C.M. Mak, Large-eddy Simulation of flow and dispersion around an isolated building: Analysis of influencing factors, Computers & Fluids 118 (2015) 89-100, https://doi.org/10.1016/j.compfluid.2015.06.006.

[60] B. Leitl, M. Schatzmann, Flow and dispersion in a finite array of rectangular buildings, 2010. http://www.mi.uni-hamburg.de/cedval.2010.

[61] R. Meroney, Wind tunnel and numerical simulation of pollution dispersion: a hybrid approach, Paper for Invited Lecture at the Croucher Advanced Study Institute, Hong Kong University of Science and Technology (2004) 6-10.

[62] Z.T. Ai, C.M. Mak, Potential use of reduced-scale models in CFD simulations to save numerical resources: Theoretical analysis and case study of flow around an isolated building, Journal of Wind

783 Engineering and Industrial Aerodynamics 134 (2014) 25-29,
784 https://doi.org/10.1016/j.jweia.2014.08.009.
785 [63] Y. Tominaga, A. Mochida, R. Yoshie, *et al.*, AIJ guidelines for practical applications of CFD to
786 pedestrian wind environment around buildings, Journal of Wind Engineering and Industrial
787 Aerodynamics 96(10-11) (2008) 1749-1761, https://doi.org/10.1016/j.jweia.2008.02.058.
788 [64] J. Franke, A. Hellsten, H. Schlünzen, *et al.*, Best practice guideline for the CFD simulation of flows
789 in the urban environment: COST Action 732 Quality Assurance and Improvement of Microscale
790 Meteorological Models, 2007.
791 [65] Fluent, ANSYS FLUENT 13.0 Theory Guide, ANSYS Inc, Canonsburg, PA, 2010.
792 [66] S.D. Sabatino, R. Buccolieri, H.R. Olesen, *et al.*, COST 732 in practice: the MUST model
793 evaluation exercise, International Journal of Environment and Pollution 44(1/2/3/4) (2011),
794 https://doi.org/10.1504/ijep.2011.038442.
795 [67] O.H.R. Schatzmann M, Franke J COST 732 Model Evaluation Case Studies: Approach and Results,
796 COST Office, Brussels, Belgium, 2010.
797 [68] S.R. Hanna, O.R. Hansen, S. Dharmavaram, FLACS CFD air quality model performance
798 evaluation with Kit Fox, MUST, Prairie Grass, and EMU observations, Atmospheric Environment
799 38(28) (2004) 4675-4687, https://doi.org/10.1016/j.atmosenv.2004.05.041.